Journal of Sol-Gel Science and Technology
https://doi.org/10.1007/s10971-020-05316-w

ORIGINAL PAPER: NANO-STRUCTURED MATERIALS (PARTICLES, FIBERS, COLLOIDS, COMPOSITES, ETC.)

The possibility of vanadium substitution on Co lattice sites in $CoFe_2O_4$ synthesized by sol–gel autocombustion method

Parvin Imanipour[1] · Saeed Hasani[1] · Amir Seifoddini[1] · Atefeh Farnia[1] · Fatemeh Karimabadi[1] · Khadijeh Jahanbani-Ardakani[2] · Fatemeh Davar[3]

Received: 4 February 2020 / Accepted: 9 May 2020
© Springer Science+Business Media, LLC, part of Springer Nature 2020

Abstract

In this study, the effect of vanadium addition on the structural and magnetic properties of cobalt ferrite ($Co_{1-x}V_xFe_2O_4$; where $x = 0$, 0.05, 0.10, 0.15, 0.20, and 0.25) prepared by a novel sol–gel autocombustion method was investigated. The formation of cubic spinel structure (space group *Fd3m*) was confirmed by X-ray diffraction in combination of Rietveld structure refinement analysis and transform infrared spectroscopic spectrum (FT-IR) analyses. Also, phase and elemental analyses confirmed that an inevitable secondary phase of hematite along with the spinel phase appears by addition of vanadium; therefore, a nanocomposite was formed in the sample containing vanadium. However, the SEM observations in combination of the results obtained by Rietveld structure refinement analysis showed that the presence of vanadium can affect the size of synthesized cobalt ferrite. VSM measurements showed that saturation magnetization and coercivity values are strongly dependent on the vanadium content and particle size, so that the maximum value of coercivity was obtained equal to ~916 Oe for $Co_{0.85}V_{0.15}Fe_2O_4$.

Graphical Abstract

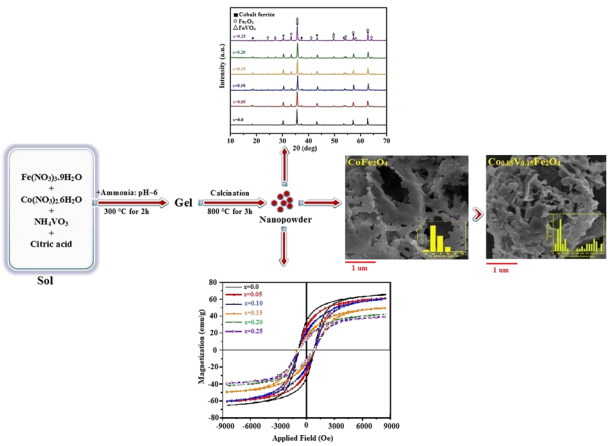

Keywords Cobalt ferrite · Nanocomposite · Rietveld refinement method · Magnetic properties · Coercivity

✉ Saeed Hasani
hasani@yazd.ac.ir

[1] Department of Mining and Metallurgical Engineering, Yazd University, 89195-741 Yazd, Iran

[2] Department of Industrial Engineering, Meybod University, Meybod, Iran

[3] Department of Chemistry, Isfahan University of Technology, Isfahan, Iran

Published online: 17 May 2020

Highlights

- Effect of vanadium ions addition on the magnetic properties of cobalt ferrite.
- Effect of adding these ions on morphology and agglomeration of the nanoparticles.
- The evolution of structural properties by using the Rietveld method.

1 Introduction

Spinel ferrites nanoparticles are known as one of the most remarkable materials in modern technology [1–4]. Among these ferrites, cobalt ferrite ($CoFe_2O_4$) has attracted the attention of numerous researchers because of its unique characteristics, such as moderate saturation magnetization (~80 emu/g) [5], high coercivity (~5400 Oe) [6], high Curie temperature (520 °C) [7, 8], significant chemical stability, and mechanical hardness [7, 9]. These unique properties make it an excellent candidate not only for various applications, such as hyperthermia [8, 10, 11], magnetic drug delivery [7, 12], magnetic resonance imaging [9, 13], medical diagnosis [12], but also for magneto-optics devices [14], high-density recording media [6, 13], and stress sensor [5]. On the other hand, these magnetic nanoparticles were synthesized by various methods such as sol–gel [1], hydrothermal [15], coprecipitation [3, 16], and microemulsion [17] methods. Among these methods, the sol–gel method has been used in numerous papers to obtain homogeneous nanoparticles [18–24].

In recent years, the effect of addition of various agents and alloying elements in order to improve the morphology and magnetic properties of cobalt ferrite nanoparticles synthesized by sol–gel method has been studied, so that it has been shown that the doping of alloying elements, such as Mg [23, 25], Ca [26], Sr [3, 27, 28], Y [1, 6], Ti [18, 29], V [30], Cr [31], Mn [32], Ni [33], Cu [19, 34], Zn [35, 36], Al [37], Dy [38, 39], and Ho [22] can significantly improve its properties. Among these doping elements, some of them enhance the soft magnetic properties, while the others increase the hard magnetic properties. For instance, it turns out to be a soft magnetic material by doping of Mg^{2+} [25] or Zn^{2+} [36] ions, while addition of alloying elements such as vanadium can increase the coercivity of cobalt ferrite [30]. Heiba et al. [30] synthesized $CoFe_{2-x}V_xO_4$ ($0 \le x \le 0.25$) and $CoFe_{2-1.67\times}V_xO_4$ ($x = 0.1$ and $x = 0.2$) by using the sol–gel method and showed that vanadium occupies on B-site for $x < 0.1$ for $CoFe_{2-x}V_xO_4$, while some of vanadium immigrates to A-site for $x > 0.1$. However, the saturation magnetization of V-doped samples was obtained less than that of for pure $CoFe_2O_4$, but coercivity increased with an increase in vanadium concentration and also an increase in magnetocrystalline anisotropy. Despite the done investigations, to the authors' knowledge, no works have been devoted to the effect of substitution of cobalt ions by vanadium on the phase evolution, size, morphology, and magnetic properties of $CoFe_2O_4$ magnetic nanoparticles prepared by sol–gel method. Therefore, it seems that more comprehensive study is necessary. Accordingly, the main objective of this study is the synthesis of the $Co_{1-x}V_xFe_2O_4$ magnetic nanoparticles by a novel sol–gel autocombustion method. For this purpose, the thermal analysis, morphological characteristics, phase analysis, and magnetic properties are investigated by simultaneous thermal analysis, field emission scanning electron microscopy (FE-SEM), X-ray diffraction (XRD), and vibrating sample magnetometer (VSM), respectively. Moreover, a comprehensive structural analysis was done using the "Rietveld refinement" method.

2 Materials and methods

2.1 Materials and synthesis process

In this study, the used raw materials including cobalt (II) nitrate hexahydrate ($Co(No_3)_2{\cdot}6H_2O$, ≥99%), iron (III) nitrate nonahydrate ($Fe(NO_3)_3{\cdot}9H_2O$, ≥99%), ammonium monovanadate (NH_4VO_3, ≥99%), citric acid (≥99.5%), and ammonia (≥25%) were obtained from Merck (Darmstadt, Germany). To investigate the effect of vanadium doping on the morphology and magnetic properties of $CoFe_2O_4$, samples with the compositions of $Co_{1-x}V_xFe_2O_4$, where $x = 0$, 0.05, 0.10, 0.15, 0.20, and 0.25 in molar ratio, were prepared by the sol–gel autocombustion method as presented in Fig. 1. For this reason, at the first stage, stoichiometric amounts of nitrate precursors and citric acid were dissolved together in a minimum amount of double distilled water at room temperature under stirring to obtain a clear solution. Then, ammonia was slowly added to this solution to adjust the pH at 6. Afterward, the solution was heated at 80 °C for 3 h with constant stirring using hot plate to achieve a viscous brown gel. At the next stage, the obtained gel was heated under stirring at 300 °C for 2 h to evaporate the solvent water and this process was followed by decomposing of the precursors in a furnace at 800 °C for 3 h under air atmosphere to get the final product.

2.2 Characterization techniques

To determine the occurred phenomena during the combustion process and formation of final product, thermal analysis of the precursors was investigated by a combined thermogravimetry/differential thermal analysis technique

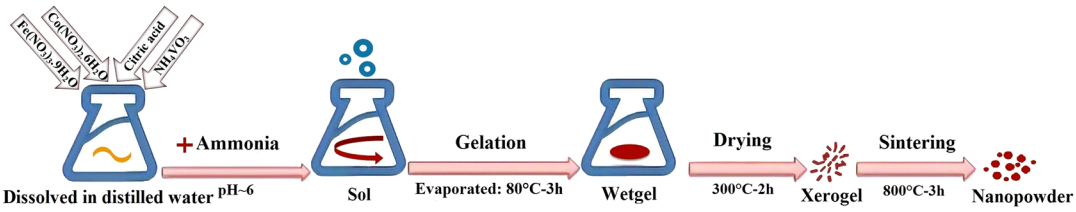

Fig. 1 Schematic representation of the sol–gel process used in the present study

(TG–DTA, STA503, Bahr, USA) up to 1200 °C at a heating rate of 20 °C/min in the air atmosphere. The diffraction patterns of the synthesized powder were obtained by XRD (PW1730 PHILIPS, Netherlands) using Cu kα radiation ($\lambda = 0.1540$ nm) and a working voltage and current of 40 kV and 30 mA, respectively. The Rietveld's powder structure refinement analysis of XRD data was adopted to obtain the relative phase abundance, particle size, and lattice parameter changes. Also, the particles size distribution and the morphology of the synthesized nanoparticles were investigated using FE-SEM equipped with energy dispersive spectroscopy (EDS) (MIRA 3, TESEAN, Czech Republic). The surface functional groups were analyzed by Fourier transform infrared spectroscopic spectrum (FT-IR, Aatar, Thermo, USA) at wave number range of 400–4000 cm^{-1}. Also, VSM (Magnetic Daghigh Daneshpajouh, Iran) was used to obtain the magnetic properties of the samples at room temperature under magnetic field up to 1 T.

3 Results and discussion

3.1 DTA–TG analysis

Figure 2 illustrates the DTA–TG curves related to the combustion process of dried gels of the samples with compositions of $Co_{1-x}V_xFe_2O_4$, where $x = 0$ and 0.15. According to TG curves, it is observed that the weight loss occurs in two stages. At the first stage, a weight loss is observed from ambient temperature up to 360 °C, which is due to both the evaporation of residual water in the gel and the removal/desorption of trapped water/other gases (i.e., N_2H_4 [40]) in the samples. Although, it seems that evaporation of residual water to be exothermic process, but some other reactions can be endothermic process at this temperature range. Therefore, no peak at this temperature can be observed on the DTA curves and this similar behavior was supported by literatures [8, 41]. At the next stage, the weight loss occurs in the temperature range of 360–430 °C, which is due to the decomposition of nitrate salts and other organic compounds, and also the formation of the spinel ferrite. As shown, the second weight loss stage is associated with the first sharp exothermic peak in the

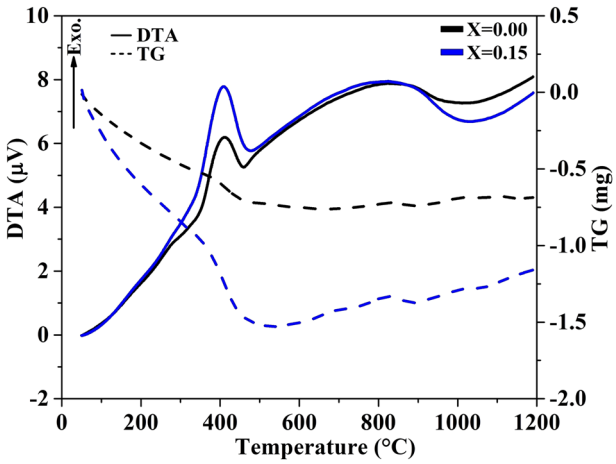

Fig. 2 DTA–TG curves of the combustion process in dried gels of the samples with compositions of $Co_{1-x}V_xFe_2O_4$, where $x = 0$ and 0.15

DTA curves for both samples. These results are in good agreement with the results obtained by others [42, 43]. However, a broad exothermic peak is shown in the temperature range of ~430–960 °C, while no weight loss is observed in TG curve in the temperature range. Therefore, this exothermic peak is attributed to the densification of the powder and this similar behavior was supported by literatures [8, 44–46]. Moreover, it should be noted that both stages of weight loss are increased in the presence of vanadium. Also, it is shown that the first DTA peak of the sample containing vanadium (0.15 at.%) is sharper than that of the vanadium-free sample, which shows that a strong combustion reaction occurs in the presence of vanadium. It can influence on the morphology, and structural and magnetic properties of the synthesized nanoparticles.

3.2 Phase and structural analysis

XRD patterns of all synthesized samples with the compositions of $Co_{1-x}V_xFe_2O_4$, where $x = 0$, 0.05, 0.10, 0.15, 0.20, and 0.25, are shown in Fig. 3. As seen, all diffraction peaks are matched properly with the standard pattern of the cubic spinel structure of $CoFe_2O_4$ (JCPDS reference card #96-591-0064). The detected diffraction peaks related to the ferrite are assigned to (111), (220), (311), (222), (400),

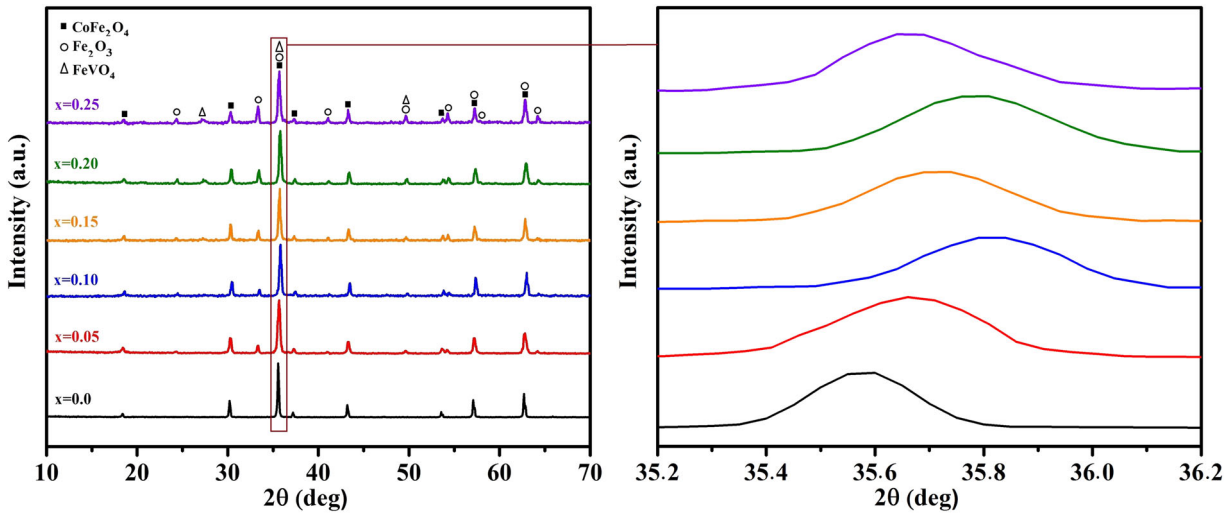

Fig. 3 XRD patterns of the synthesized samples with compositions of $Co_{1-x}V_xFe_2O_4$ ($0 \le x \le 0.25$) sintered at 800 °C/3 h

Table 1 Chemical composition, microstructural, and morphological properties of $Co_{1-x}Fe_2V_xO_4$ ($x = 0$, 0.05, 0.10, 0.15, 0.20, and 0.25) samples

Sample no.	Chemical composition	Crystallite size (nm)			wt%	X-ray density (g/cm^3)	Lattice parameter (Å)		Volume (Å^3)
		XRD					Rietveld analysis	XRD	
		Debye–Scherrer's formula	Rietveld analysis	FE-SEM	Rietveld analysis				
1	$CoFe_2O_4$	51.4	74.3	91	100	5.32	8.39275	8.364	585.1
2	$Co_{0.95}V_{0.05}Fe_2O_4$	31.6	39.5	135	81.5	5.36	8.38782	8.337	579.5
3	$Co_{0.90}V_{0.10}Fe_2O_4$	35.8	48.5	326.9	74.6	5.42	8.38142	8.304	572.6
4	$Co_{0.85}V_{0.15}Fe_2O_4$	41.1	58.7	594	71.6	5.34	8.38635	8.341	580.3
5	$Co_{0.80}Fe_2V_{0.20}O_4$	34.3	42.3	–	62	5.35	8.38748	8.328	577.6
6	$Co_{0.75}V_{0.25}Fe_2O_4$	27.4	44.4	–	53.9	5.29	8.38282	8.355	583.2

(422), (511), and (440) planes at 2θ values of 18.389°, 30.250°, 35.632°, 37.274°, 43.309°, 53.736°, 57.286°, and 62.913°, respectively. Therefore, it is a clear evidence for the formation of cobalt ferrite in all samples. However, in addition to this phase, two other phases are also found in the samples containing vanadium, which are assigned to the hematite (Fe_2O_3; JCPDS reference card #96-591-0083) and the iron vanadium oxide ($FeVO_4$; JCPDS reference card #00-030-0667) phases. As shown, the diffraction peaks of these phases become broader and sharper by adding more vanadium. It means that the volume factions of these two phases are increased with an increase in the amount of vanadium. Although the main purpose of this work is to investigate the effect of substitution of vanadium for cobalt in the cobalt ferrite structure, the XRD patterns show that this substitution is limited. Thus, other phases including Fe_2O_3 and $FeVO_4$ are formed in the presence of vanadium and the relative amount of these secondary phases is increased by an increase in vanadium amount. Similar results are observed for substitution of Er [47] and Ho [22] for cobalt in the cobalt ferrite structure.

Heiba et al. [30] reported that V can be substituted as the V^{5+} or/and V^{3+} ions. However, in the present study, NH_4VO_3 was used as the source of vanadium +5 cations. Although the occupation of the octahedral sites (B sites) by V^{5+} ions at low concentration of vanadium has been reported, some researchers believe that the size of the V^{5+} (0.36 Å) is smaller than the Fe^{3+} (0.64 Å) and Co^{2+} (0.78 Å) ions, so that V^{5+} ions tend to occupy the tetrahedral sites (A-sites) [48]. However, it seems that the occupation of a significant amount of Co^{2+} by V^{5+} cannot be occurred and V^{5+} ions occupy the Fe sites, and therefore Fe^{3+} ions can form other secondary phases, i.e., Fe_2O_3 and $FeVO_4$, which is confirmed by the XRD patterns.

The average crystallite size of cobalt ferrite formed in all samples is calculated using the Scherer's formula [49]

$$D = \frac{0.9\lambda}{\beta \mathrm{Cos}\theta}, \quad (1)$$

where β is the full width at half maximum, and λ is the X-ray wavelength (0.1540 nm) [50]. The calculated average crystallite size for all samples is summarized in Table 1. As

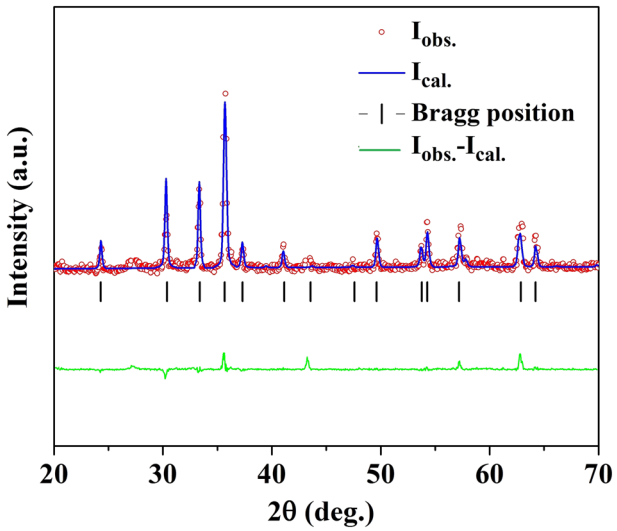

Fig. 4 Rietveld refined XRD patterns for the sample containing 0.25 at.% V

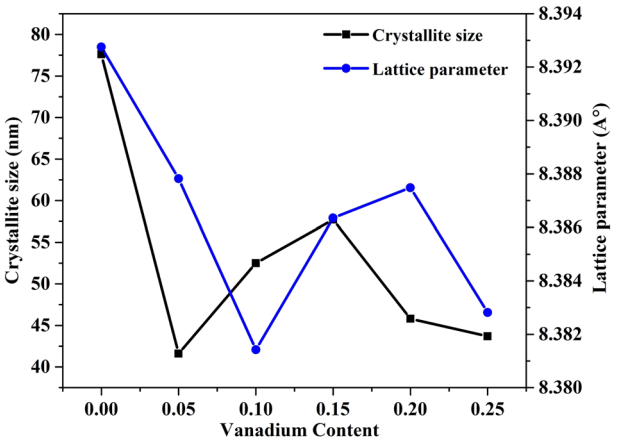

Fig. 5 The average crystallite size and lattice parameter with vanadium content for $x = 0$–0.25

seen, the calculated average crystallite size decreases from ~51 nm ($CoFe_2O_4$) to ~27 nm ($Co_{0.75}V_{0.25}$ Fe_2O_4). However, it is obvious that the average crystallite size of cobalt ferrite nanoparticles in the presence of vanadium is smaller than that of V-free $CoFe_2O_4$.

On the other hand, a careful XRD analysis (Fig. 3) reveals the shift of diffraction peaks, which indicates a change in the lattice parameter. Therefore, the lattice parameters are calculated using the following equation [36]:

$$a = d_{hkl}\sqrt{h^2 + k^2 + l^2}, \tag{2}$$

where d is the interplanar spacing; a is the lattice parameter; and (hkl) are Miller indices of the diffraction peaks. Moreover, the unit cell volume of the synthesized nanoparticles is calculated using the formula expressed as follows:

$$V = a^3, \tag{3}$$

where a represented the lattice parameter calculated using Eq. (2).

Values of the calculated lattice parameter and the unit cell volume are presented in Table 1.

As mentioned, the size of V^{5+} ion is smaller than that of the Fe^{3+} (0.64 Å) and Co^{2+} (0.78 Å) ions. Therefore, the lattice parameter and the unit cell volume of synthesized cobalt ferrite decrease by addition of vanadium, which can be due to a partial substitution of smaller vanadium ions instead of iron and/or cobalt ions. Also, all the XRD patterns were refined by using the Rietveld method to evaluate the average crystallite size and lattice parameters (Table 1). As seen, there is a good agreement between the structural parameters calculated by both the Scherer's formula and the Rietveld method. For instance, Fig. 4 shows the measured XRD patterns based on the Rietveld refinement technique for the sample containing 0.25 at.% V. However, as seen in Table 1, the crystallite sizes evaluated from Rietveld analysis are larger than those obtained from Scherrer's formula. In is notable that in Rietveld analysis, refinement is done by using all peaks, while for those obtained from Scherrer's formula, only (220) peak was considered, because the peaks of secondary phase overlapped with other cobalt ferrite peaks. Also, Fig. 5 indicates the relation between the lattice parameter and the average crystallite size calculated by the Rietveld method versus vanadium content. As seen, both structural parameters in V-free sample are higher than samples containing V, which can be due to the smaller vanadium ions as compared with both iron and cobalt ions. On the other hand, not only ionic radius but also the average grain size can affect the lattice parameter. It is reported that smaller particles have large surface area as well as high surface tension [51]. As seen in Fig. 5, the lattice parameter and the average crystallite size are in good agreement with each other. Therefore, the decrease in lattice parameter suggests possible lattice shrinkage due to the high surface tension of smaller particles. The similar behavior was shown in the literatures [35, 51].

On the other hand, NH_4VO_3 is known as a source of the vanadium +5 oxidation states. Therefore, V occupies the lattice sites as V^{5+}. It is acceptable that small ions with high charges occupy the tetrahedral sites [30]. The V^{5+} ion radius is small compared with Co^{2+}, Fe^{2+}, and Fe^{3+} ions, therefore V^{5+} ions tend to occupy the tetrahedral sites [52, 53]. Nevertheless, it is reported that V^{5+} ions may occupy the octahedral sites at low concentration of vanadium [48, 54]. Accordingly, V^{5+} adding into the lattice sites results in the creation of some Fe^{2+}, so that each V^{5+} ion

converts two Fe^{3+} ions into two Fe^{2+}. Therefore, Fe^{2+} ions are formed due to the incorporation of V^{5+} into the lattice [55]. The similar behavior has been reported in the case of Ti^{4+}–Fe^{2+} pairs in the titanium substituted Mn–Zn ferrite [56].

As mentioned, if V^{5+} ions occupy the octahedral sites at low concentration of vanadium (<0.15), it can lead to decrease in the lattice parameter. But, in the samples with vanadium content > 0.15, a significant part of vanadium ions occupy the tetrahedral sites as V^{5+} ions, that it can lead to enlarge the cell. Although V^{5+} ions have a smaller radius than Fe^{3+} ions, this incorporation into the lattice results in the creation of some Fe^{2+} that have a longer ionic radius compared with Fe^{3+} ions. So, this can lead to a slight increase in the lattice parameter for the samples with vanadium content > 0.15. On the other hand, as observed in XRD patterns, it is shown that driving force of the formation of secondary phases (i.e., Fe_2O_3) is increased by more addition of vanadium, so it can be expected that in the presence of high concentration of vanadium (0.25), formation of secondary phases leads to a decrease in lattice parameter of cobalt ferrite. It should be noted that some Co^{2+} sites may be substituted by V^{5+} ions. This can lead to the exit of a divalent (Co^{2+}/Fe^{+2}) and trivalent ion (Fe^{3+}) from the structure. Therefore, formation of the secondary phases (i.e., Fe_2O_3) can be expected. Furthermore, it is also possible that some of the vanadium ions cannot substitute the sites of unit cell of $CoFe_2O_4$ and appear in the secondary phases (i.e., $FeVO_4$).

Furthermore, the X-ray density is calculated for all the samples by using the following equation [57, 58]:

$$\rho_{\text{th}} = \frac{8 \cdot M}{N_a \cdot a^3}, \tag{4}$$

where M is the molecular weight; a represents the lattice parameters; 8 is the number of molecules per unit cell of cubic spinel lattice; and N is the Avogadro number. Figure 6 illustrates the variation of unit cell volume and X-ray density versus vanadium concentration. As seen, it is clear that the X-ray density increases by vanadium doping ($x = 0.1$), while this parameter reduces by adding more vanadium, which is in good agreement with the effect of vanadium doping on the lattice parameter/unit cell volume.

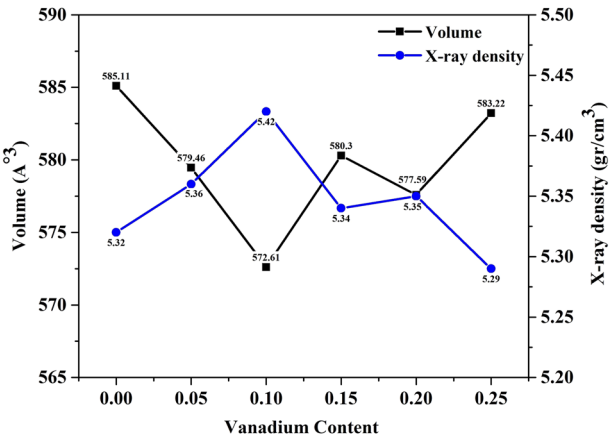

Fig. 6 The variation of volume of unit cell and theoretical density for $Co_{1-x}V_xFe_2O_4$ with increasing vanadium content

3.3 Microstructural observations

Figure 7 represents the FE-SEM images and the particle size distribution of the synthesized samples with the compositions of $Co_{1-x}V_xFe_2O_4$ ($x = 0$, 0.05, 0.10, and 0.15). As shown, there are significant differences in the morphology and the average crystallite size of the synthesized nanoparticles in the presence of various amount of vanadium. As seen, the nanoparticles of the V-free sample have an agglomerated semispherical morphology (Fig. 7a). But, the shape of some of the synthesized nanoparticles differs from a semispherical morphology in the V-free sample to a cubical shape by addition of 0.05 at.% V (Fig. 7b). This may happen due to the presence of hematite phase and magnetic interaction, so that this interaction produces a low surface energy state and reduces the interface between nanoparticles [59]. On the other hand, the particles size of $Co_{0.9}V_{0.1}Fe_2O_4$ sample was increased (Fig. 7c). Figure 7d shows that there are two different morphologies in the sample containing 0.15 at.% V. In order to confirm the chemical composition of these synthesized particles, an EDS study was carried out. Typical EDS patterns of the samples containing 0.05 and 0.15 at.% V are shown in Fig. 7f–i. Also, the stoichiometry of the formed phase with the theoretical one in EDS patterns are compared in Table 2 to better understand the possibility of substitution of vanadium on sites of $CoFe_2O_4$. As seen, it is accepted that some vanadium ions occupy the sites of $CoFe_2O_4$.

Moreover, the average of particle size calculated by MIP is presented in Table 1. As presented, the values of particle size measured by using the FE-SEM micrographs is larger than those obtained from XRD patterns; it is due to the fact that every particle is formed by aggregation of a large number of crystallites [60, 61].

3.4 FT-IR analysis

The FT-IR spectroscopy is a useful method to determine the chemical functional groups and structural changes occurring in materials [35]. Figure 8 represents the FT-IR absorption spectra of the synthesized samples with compositions of $Co_{1-x}V_xFe_2O_4$, where $x = 0$, 0.05, 0.10, 0.15, 0.20, and 0.25. As seen, the spectra are made up of two basis strong fundamental stretching vibrations in the ranges of

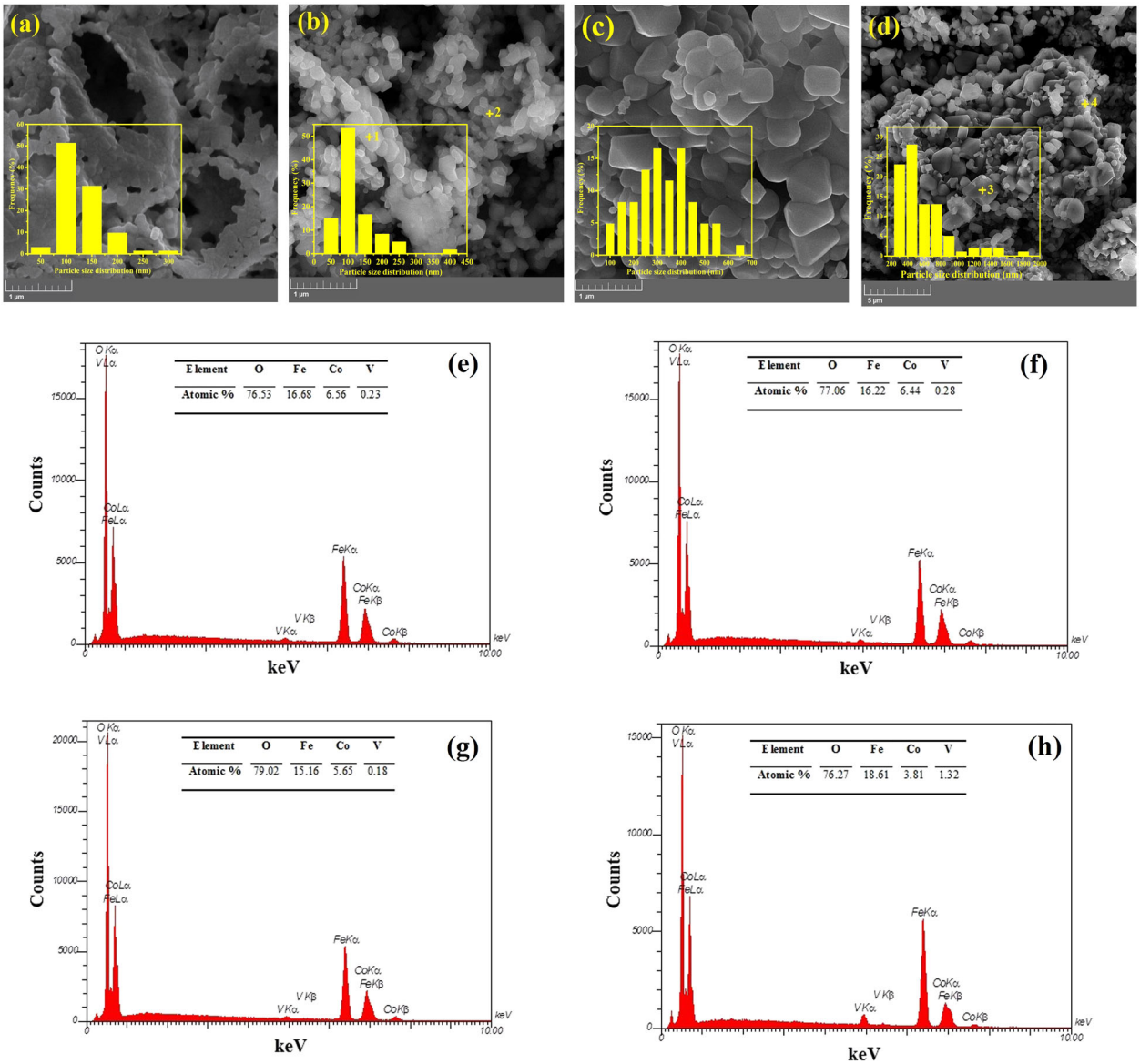

Fig. 7 FE-SEM images of the synthesized samples with the compositions of $Co_{1-x}V_xFe_2O_4$, where $x = 0$ (**a**), 0.05 (**b**), 0.10 (**c**), and 0.15 at.% (**d**). EDS patterns related to the points 1 (**e**), 2 (**f**), 3 (**g**), and 4 (**h**) shown in **b** and **d**

Table 2 Elemental composition of the synthesized nanoparticles of $Co_{1-x}V_xFe_2O_4$ ($x = 0.05$ and 0.15) as evaluated from stoichiometry composition and EDS

Elemental composition evaluated from	Co (at.%)	Fe (at.%)	O (at.%)	V (at.%)
Stoichiometry composition				
$CoFe_2O_4$	14.29	28.57	57.14	0
$Co_{0.95}V_{0.05}Fe_2O_4$	13.57	28.57	57.14	0.72
$Co_{0.85}V_{0.15}Fe_2O_4$	12.14	28.57	57.14	2.15
EDS				
Point 1	6.56	16.68	76.53	0.23
Point 2	6.44	16.22	77.06	0.28
Point 3	5.65	15.16	79.02	0.18
Point 4	3.81	18.61	76.27	1.32

500–460 cm^{-1} (υ_A) and 600–500 cm^{-1} (υ_B), which are related to the tetrahedral and octahedral sites of the spinel structure, respectively. The differences in vibrations frequencies between the two crystallographic A and B sites can be ascribed to the transition in bond length (M–O), where the ionic radius of A-site is smaller than that of B-site [59]. Also, there are the peaks at 1090 and 1382 cm^{-1}, which are related to the C–O and asymmetrical COO– groups, respectively [2]. Furthermore, the FT-IR spectra of the samples display bands at 1630 cm^{-1}, which are attributed to bending and stretching vibration of H–O–H [39]. Moreover, the bands at 2923 cm^{-1} are assigned to the vibration mode of the C–H bond [2, 62], and also the bands

at 3420 cm^{-1} are attributed to the O–H bond [63]. As summarized, it is clear that the addition of vanadium can effect on the migration of the cations between the tetrahedral and octahedral sites.

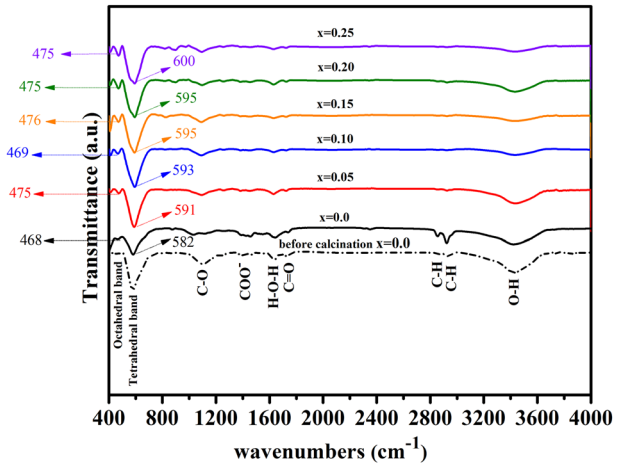

Fig. 8 FT-IR spectra of the samples with the compositions of $Co_{1-x}V_xFe_2O_4$, where $0 \le x$ (at.%) ≤ 0.25

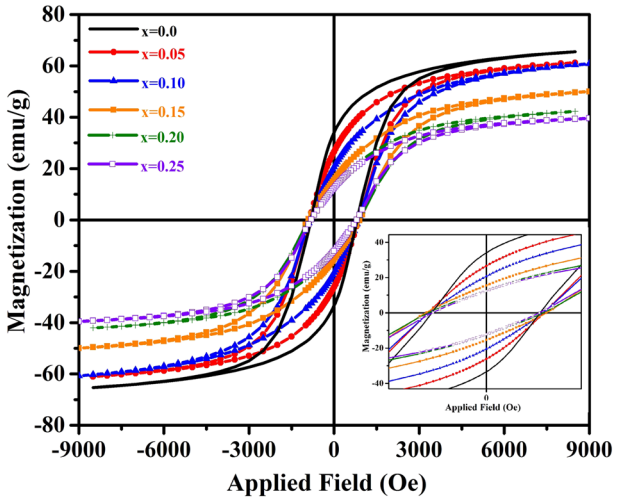

Fig. 9 Hysteresis loops for all the compositions ($Co_{1-x}V_xFe_2O_4$, where $0 \le x$ (at.%) ≤ 0.25) at room temperature

3.5 VSM measurements

Figure 9 depicts the hysteresis loops for all the samples, which shows the effect of presence of vanadium on the magnetic behavior of the cobalt ferrite. Magnetic characteristics including saturation magnetization (M_s), coercivity (H_c), and remanent magnetization (M_r) for all synthesized samples are extracted from the hysteresis loops and are summarized in Table 3. Also, variation of the M_s and H_c with vanadium content is shown in Fig. 10. As seen, M_s decreases by adding vanadium, which is due to the appearance of nonferromagnetic secondary phases (Fe_2O_3 and $FeVO_4$). Also, the experimental magnetic moment (n_B in Bohr magneton) has been calculated from the M_s value using the following equation [38, 64, 65] and the results are presented in Table 3:

$$\mu_B = \frac{M_{CoFe_2O_4} \times M_s}{5585}, \tag{5}$$

where $M_{CoFe_2O_4}$ is the molecular weight of particular ferrite composition, and M_s is saturation magnetization (emu/g). As presented, the changes in the saturation magnetization and the magnetic moment are in good agreement with each other, which is related to the appearance of secondary phases.

On the other hand, as presented in Table 3, the variation of M_s, M_r, n_B, K, and M_r/M_s are monotonic, while the variation of H_c is not monotonic. The coercivity, an important magnetic property, is affected by various factors, i.e., the structural defects, the average crystallites size, the appearance of secondary phases, the magnetocrystalline anisotropy (K), etc. [30, 66]. For instance, the coercivity is the required magnetic field for overcoming the magnetocrystalline anisotropy to flip the magnetic moments. Therefore, the change in anisotropy field by adding vanadium can change the coercivity. The anisotropy for all samples is calculated by the following formula [57, 65]:

$$K = \frac{H_c \times M_s}{0.98}, \tag{6}$$

here, M_s and H_c represent the saturation magnetization and coercivity, respectively. Values of the calculated anisotropy are summarized in Table 3. Moreover, this sudden change

Table 3 Magnetic properties of $Co_{1-x}Fe_2V_xO_4$ (with $x = 0$, 0.05, 0.10, 0.15, 0.20, and 0.25) samples

Sample no.	Vanadium content	M_s (emu/g)	M_r (emu/g)	H_c (Oe)	K × 10^4 (erg/g)	n_B	M_r/M_s
1	–	65.6	33.9	820.3	5.50	2.75	0.51
2	0.05	61.3	26.6	880.1	5.50	2.57	0.43
3	0.10	60.6	20.5	859.7	5.31	2.53	0.33
4	0.15	49.6	15.5	915.8	4.63	2.07	0.31
5	0.20	42.3	12.9	875.6	3.77	1.76	0.30
6	0.25	39.4	12.3	809.7	3.25	1.64	0.31

in magnetic behavior of cobalt ferrite by adding vanadium can be related to the possible change in orientation of the magnetization vector from the easy axis (100) to the hard axis (111) in $CoFe_2O_4$ [67]. On the other hand, as mentioned before, the coercivity can be affected simultaneously by various factors. Hence, a nonmonotonic variation for this parameter can be expected. While, the main reason of the change in other magnetic parameters is the presence of secondary phases, which are formed by addition of V.

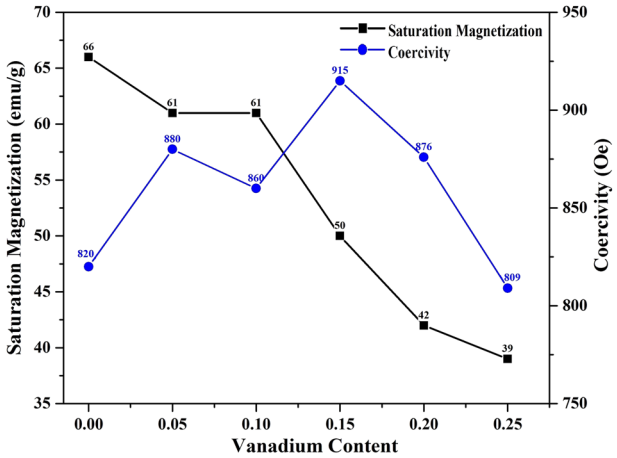

Fig. 10 Variation of coercivity and saturation magnetization as a function of vanadium content

Furthermore, the obtained magnetic parameters for cobalt ferrites synthesized in the present work and the other studies [22, 25, 26, 30, 31, 33, 35, 38, 41, 68] are compared in Table 4. As shown, $CoFe_2O_4$ synthesized in the present work has magnetic properties better than that obtained in most of the previous works.

4 Conclusion

In the present study, the effect of vanadium addition on the size, morphology, phase evolution, and magnetic properties of magnetic $CoFe_2O_4$ nanoparticles synthesized by a novel sol–gel autocombustion method was investigated. The obtained results revealed the following:

(1) The vanadium atoms cannot be completely substituted by cobalt atoms sites; therefore, two other phases were also found in the samples containing vanadium. However, Rietveld structure refinement analysis

Table 4 The average of crystallite size and magnetic properties of $CoFe_2O_4$ MNPs in comparison to other investigations [22, 25, 26, 30, 31, 33, 35, 38, 41, 68]

Chemical composition	Crystallite size (nm)	M_s (emu/g)	H_c (Oe)	M_r (emu/g)	Ref.
Substitution for iron					
$CoFe_{2-x}Ho_xO_4$ ($x = 0.0, 0.05, 0.10, 0.15, 0.20$)	64.4–75.8	49.7–65	440.7–618.8	16–24.1	[22]
$CoFe_{2-x}Cr_xO_4$ ($x = 0.0, 0.2, 0.4, 0.6, 0.8, 1.0$)	13.9–27.8	49.7–115.7	302–1428.4	7.4–92.6	[31]
$CoFe_{2-x}Dy_xO_4$ ($x = 0.025, 0.05, 0.075, 0.10$)	4.1–13	9.7–14	21.3–312.8	0.24–3.3	[38]
$CoFe_{2-x}V_xO_4$ ($x = 0.0, 0.05, 0.10, 0.15, 0.20, 0.25$) $CoFe_{2-1.67\times}V_xO_4$ ($x = 0.10, 0.20$)	18–106	63.2–83.5	870.4–2476.6	25.7–39.4	[30]
Substitution for cobalt					
$Co_{1-x}Mg_xFe_2O_4$ ($x = 0.0, 0.2, 0.4, 0.6, 0.8, 1.0$)	50.8–66.8	35.2–77.9	38.3–680.2	4.9–23.2	[25]
$Co_{1-x}Ca_xFe_2O_4$ ($x = 0.0, 0.05, 0.10, 0.15$)	42.9–71.8	43.2–63.9	819.8–1312.1	17.2–26	[26]
$Co_{1-x}Ni_xFe_2O_4$ ($x = 0.1, 0.3, 0.5, 0.7, 0.9$)	70–160	37.3–70.8	321–1188	–	[33]
$Co_{1-x}Zn_xFe_2O_4$ (0.0, 0.5)	21.7–41.5	21.4–65.7	9.6–47.5	0.36–18.8	[35]
$Co_{1-x}Cu_xFe_2O_4$ (0.0, 0.05, 0.10, 0.15, 0.20, 0.25)	40.4–45.8	74–82.6	1121.3–1281.5	31.5–36.8	[41]
$Co_{1-x}Ni_xFe_2O_4$ ($x = 0.0, 0.25, 0.5, 0.75, 1.0$)	23–27	41.7–76.1	162.5–1049.6	12.1–36.3	[68]
$Co_{1-x}V_xFe_2O_4$ ($x = 0.0, 0.05, 0.10, 0.15, 0.20, 0.25$)	27.4–51.4	39.4–65.6	809.7–915.8	12.3–33.9	This work

confirmed that the addition of vanadium affects both the average crystallite size and the lattice parameter of the synthesized cobalt ferrite nanoparticles.

(2) The formation of the secondary phases such as Fe_2O_3 was confirmed by FE-SEM observations.

(3) The functional group was studied by FT-IR analysis, which confirmed the formation of cubic spinel phase in all samples.

(4) The saturation magnetization was decreased by addition of vanadium due to the formation of secondary phases. While, the coercivity was increased from 823 Oe in the vanadium-free sample to 918 Oe in the samples with composition of $Co_{0.85}V_{0.15}Fe_2O_4$. The increase in the coercivity was correlated with the presence of secondary phases, the average crystallites size changes, and the magnetocrystalline anisotropy.

Compliance with ethical standards

Conflict of interest The authors declare that they have no conflict of interest.

Publisher's note Springer Nature remains neutral with regard to jurisdictional claims in published maps and institutional affiliations.

References

1. Shobana MK, Kwon H, Choe H (2012) Structural studies on the yttrium-doped cobalt ferrite powders synthesized by sol-gel combustion method. J Magn Magn Mater 324:2245–2248
2. Afshari M, Rouhani Isfahani A, Hasani S, Davar F, Jahanbani Ardakani K (2019) Effect of apple cider vinegar agent on the microstructure, phase evolution, and magnetic properties of CoFe2O4 magnetic nanoparticles. Int J Appl Ceram Technol 16:1612–1621
3. Xie T, Xu L, Liu C (2012) Synthesis and properties of composite magnetic material SrCoxFe12-xO 19 (x=0-0.3). Powder Technol 232:87–92
4. Rouhani AR, Esmaeil-Khanian AH, Davar F, Hasani S (2018) The effect of agarose content on the morphology, phase evolution, and magnetic properties of CoFe 2 O 4 nanoparticles prepared by sol-gel autocombustion method. Int J Appl Ceram Technol 15:758–765
5. Ayyappan S, Philip J, Raj B (2009) A facile method to control the size and magnetic properties of CoFe2O4 nanoparticles. Mater Chem Phys 115:712–717
6. Meng X et al. (2009) Mössbauer study of cobalt ferrite nanocrystals substituted with rare-earth Y3+ions. J Magn Magn Mater 321:1155–1158
7. Mohamed RM, Rashad MM, Haraz FA, Sigmund W (2010) Structure and magnetic properties of nanocrystalline cobalt ferrite powders synthesized using organic acid precursor method. J Magn Magn Mater 332:2058–2064
8. Zubair A et al. (2017) Structural, morphological and magnetic properties of Eu-doped CoFe2O4nano-ferrites. Results Phys 7:3203–3208
9. Senthil VP et al. (2018) Study of structural and magnetic properties of cobalt ferrite (CoFe2O4) nanostructures. Chem Phys Lett 695:19–23
10. Lima AC et al. (2015) The effect of Sr2+ on the structure and magnetic properties of nanocrystalline cobalt ferrite. Mater Lett 145:56–58
11. Sharifi I, Shokrollahi H (2012) Nanostructural, magnetic and Mössbauer studies of nanosized Co1-xZnxFe2O4synthesized by co-precipitation. J Magn Magn Mater 324:2397–2403
12. Gabal MA, Al-Juaid AA, El-Rashed S, Hussein MA (2017) Synthesis and characterization of nano-sized CoFe2O4via facile methods: a comparative study. Mater Res Bull 89:68–78
13. Amiri S, Shokrollahi H (2013) The role of cobalt ferrite magnetic nanoparticles in medical science. Mater Sci Eng C 33:1–8
14. Chae KP, Lee JG, Kim WK, Lee YB (2002) Magnetic properties of ti-doped CoFe2O4 films. J Magn Magn Mater 248:236–240
15. Ansari SM et al. (2018) Controlled surface/interface structure and spin enabled superior properties and biocompatibility of cobalt ferrite nanoparticles. Appl Surf Sci 459:788–801
16. Amiri S, Shokrollahi H (2013) Magnetic and structural properties of RE doped Co-ferrite (RE=Nd, Eu, and Gd) nanoparticles synthesized by co-precipitation. J Magn Magn Mater 345:18–23
17. Sharifi I, Shokrollahi H, Doroodmand MM, Safi R (2012) Magnetic and structural studies on CoFe 2O 4 nanoparticles synthesized by co-precipitation, normal micelles and reverse micelles methods. J Magn Magn Mater 324:1854–1861
18. Chae KP, Lee JG, Kweon HS, Lee YB (2004) The crystallographic, magnetic properties of Al, Ti doped CoFe2O4-powders grown by sol-gel method. J Magn Magn Mater 283:103–108
19. Sanpo N, Wang J, Berndt CC (2013) Sol-gel synthesized copper-substituted cobalt ferrite nanoparticles for biomedical applications. J Nano Res 22:95–106
20. Ji G, Tang S, Xu B, Gu B, Du Y (2003) Synthesis of CoFe2O4 nanowire arrays by sol-gel template method. Chem Phys Lett 379:484–489
21. Toksha BG, Shirsath SE, Patange SM, Jadhav KM (2008) Structural investigations and magnetic properties of cobalt ferrite nanoparticles prepared by sol–gel auto combustion method. Solid State Commun 147:479–483
22. Patankar KK, Ghone DM, Mathe VL, Kaushik SD (2018) Structural and physical property study of sol–gel synthesized CoFe2-xHoxO4 nano ferrites. J Magn Magn Mater 454:71–77
23. Ramakrishna A, Murali N, Mammo TW, Samatha K, Veeraiah V (2018) Structural and DC electrical resistivity, magnetic properties of Co0.5M0.5Fe2O4(M = Ni, Zn, and Mg) ferrite nanoparticles. Phys B Condens Matter 534:134–140
24. Sajjia M, Benyounis KY, Olabi AG (2012) The simulation and optimization of heat treatment of cobalt ferrite nanoparticles prepared by the sol–gel technique. Powder Technol 222:143–151
25. Mund HS, Ahuja BL (2017) Structural and magnetic properties of Mg doped cobalt ferrite nano particles prepared by sol-gel method. Mater Res Bull 85:228–233
26. Gowreesan S, Kumar AR (2018) Synthesis, structural, dielectric and magnetic properties of spinel structure of Ca2+substitute in Cobalt ferrites (Co1−xCaxFe2O4). Chin J Phys 56:1262–1272
27. Kumar R, Kar M (2016) Lattice strain induced magnetism in substituted nanocrystalline cobalt ferrite. J Magn Magn Mater 416:335–341
28. Ghasemi A (2015) Compositional dependence of magnetization reversal mechanism, magnetic interaction and Curie temperature of Co1-xSrxFe2O4 spinel thin film. J Alloy Compd 645:467–477
29. Chae KP, Kim WK, Lee JG, Lee YB (2001) Magnetic properties of Ti-doped ultrafine CoFe2O4 powder grown by the sol gel method. Hyperfine Interact 136–137:65–72
30. Heiba ZK, Mohamed MB, Ahmed SI (2017) Cation distribution correlated with magnetic properties of cobalt ferrite nanoparticles defective by vanadium doping. J Magn Magn Mater 441:409–416

31. Balavijayalakshmi J, Sudha T (2017) Effect of Cr3+ substitution on structural and magnetic properties of magnesium ferrite nanoparticles. Springe Proc Phys 189:289–297
32. Ansari MMN, Khan S (2017) Structural, electrical and optical properties of sol-gel synthesized cobalt substituted MnFe2O4nanoparticles. Phys B Condens Matter 520:21–27
33. Mozaffari M, Amighian J, Darsheshdar E (2014) Magnetic and structural studies of nickel-substituted cobalt ferrite nanoparticles, synthesized by the sol-gel method. J Magn Magn Mater 350:19–22
34. Chandra Sekhar B et al. (2016) Magnetic and magnetostrictive properties of Cu substituted Co-ferrites. J Magn Magn Mater 398:59–63
35. Yadav RS et al. (2015) Magnetic properties of Co1−x Znx Fe2 O4 spinel ferrite nanoparticles synthesized by starch-assisted sol–gel autocombustion method and its ball milling. J Magn Magn Mater 378:190–199
36. Ben Ali M et al. (2016) Effect of zinc concentration on the structural and magnetic properties of mixed Co-Zn ferrites nanoparticles synthesized by sol/gel method. J Magn Magn Mater 398:20–25
37. Zandi Khajeh MA, Shokrollahi H, Avazpour L, Toroghinejad MR (2015) Study on the effect of sol–gel parameters using the Taguchi technique to achieve the optimal crystallite size and magnetic properties of cobalt ferrite powders. J Sol-Gel Sci Technol 76:271–278
38. Yadav RS et al. (2015) Magnetic properties of dysprosium-doped cobalt ferrite nanoparticles synthesized by starch-assisted sol-gel auto-combustion method. J Supercond Nov Magn 28:2097–2107
39. Karimi Z et al. (2014) Magnetic and structural properties of nano sized Dy-doped cobalt ferrite synthesized by co-precipitation. J Magn Magn Mater 361:150–156
40. Gonsalves LR, Mojumdar SC, Verenkar VMS (2011) Synthesis and characterization of Co0.8Zn0.2Fe2O4 nanoparticles. J Therm Anal Calorim 104:869–873
41. Naik CC, Gaonkar SK, Furtado I, Salker AV (2018) Effect of Cu2+ substitution on structural, magnetic and dielectric properties of cobalt ferrite with its enhanced antimicrobial property. J Mater Sci Mater Electron 29:14746–14761
42. Kumari S, Kumar V, Kumar P, Kar M, Kumar L (2015) Structural and magnetic properties of nanocrystalline yttrium substituted cobalt ferrite synthesized by the citrate precursor technique. Adv Powder Technol 26:213–223
43. Ranjani M, Jesurani S, Priyadharshini M, Vennila S (2016) Sol-gel synthesis and characterization of zinc substituted cobalt ferrite magnetic nanoparticles. Int J Eng Res Technol 5:882–886
44. Falsafi F et al. (2017) Sm-doped cobalt ferrite nanoparticles: a novel sensing material for conductometric hydrogen leak sensor. Ceram Int 43:1029–1037
45. Rajput AB, Hazra S, Ghosh NN (2013) Synthesis and characterisation of pure single-phase CoFe2O4 nanopowder via a simple aqueous solution-based EDTA-precursor route. J Exp Nanosci 8:629–639
46. Hashemi SM, Hasani S, Jahanbani Ardakani K, Davar F (2019) The effect of simultaneous addition of ethylene glycol and agarose on the structural and magnetic properties of CoFe2O4 nanoparticles prepared by the sol-gel auto-combustion method. J Magn Magn Mater 492:165714
47. Prathapani S, Vinitha M, Jayaraman TV, Das D (2014) Effect of Er doping on the structural and magnetic properties of cobalt-ferrite. J Appl Phys 115:1–4
48. Maisnam M et al. (2004) Magnetic properties of vanadium-substituted lithium zinc titanium ferrite. Mater Lett 58:2412–2414
49. Cullity BD (1978) Elements of X-ray diffraction, 2nd edn. Addison-Wesley Publishing Co. Reading, MA
50. Scherrer P (1918) Determination of size and inner structure of colloidal particles by X-ray (Bestimmung der Grösse und der inneren Struktur von Kolloidteilchen mittels Röntgenstrahlen). Nachrichten von der Gesellschaft der Wissenschaften zu Göttingen. Math. Phys. Kl 1918:98–100
51. Šepelák V, Tkáčová K, Boldyrev VV, Wiβmann S, Becker KD (1997) Mechanically induced cation redistribution in ZnFe2O4 and its thermal stability. Phys B Condens Matter 234–236:617–619
52. Jain GC, Das BK, Tripathi RB, Narayan R (1979) Influence of V2O5 on the densification and the magnetic properties of Ni—Zn ferrite. J Magn Magn Mater 14:80–86
53. Bachmann HG, Barnes WH (1961) Bonding in the trigonal bipyramidal coordination polyhedra of V2O5 and of certain other structures containing pentavalent vanadium. Z für Krist 115:215–230
54. Kaiser M (2010) Magnetic and dielectric properties of low vanadium doped nickel–zinc–copper ferrites. J Phys Chem Solids 71:1451–1457
55. Jain G, Das B, Tripathi R, Narayan R (1982) Influence of V2O5 addition on electrical conductivity and magnetic properties of Ni-Zn ferrites. IEEE Trans Magn 18:776–778
56. Hanke I, Zenger M (1977) Mn-Zn-ferrite MIT Sn/Ti-mischsubstitution Mn-Zn ferrites with combined Sn-Ti substitutions. J Magn Magn Mater 4:120–128
57. Anjum S, Tufail R, Rashid K, Zia R, Riaz S (2017) Effect of cobalt doping on crystallinity, stability, magnetic and optical properties of magnetic iron oxide nano-particles. J Magn Magn Mater 432:198–207
58. Kulal SR et al. (2012) Synthesis of Dy doped Co-Zn ferrite by sol-gel auto combustion method and its characterization. Mater Lett 84:169–172
59. Hashhash A, Kaiser M (2015) Influence of Ce-substitution on structural, magnetic and electrical properties of cobalt ferrite nanoparticles. J Electron Mater 45:462–472
60. Mazen SA, Abu-Elsaad NI, Nawara AS (2015) Influence of silicon substitution and annealing temperature on the microstructure and magnetic properties of lithium ferrite. J Alloy Compd 648:690–697
61. Yadav RS et al. (2015) Magnetic properties of Co1-xZnxFe2O4spinel ferrite nanoparticles synthesized by starch-assisted sol-gel autocombustion method and its ball milling. J Magn Magn Mater 378:190–199
62. Topkaya R, Baykal A, Demir A (2013) Yafet-Kittel-type magnetic order in Zn-substituted cobalt ferrite nanoparticles with uniaxial anisotropy. J Nanoparticle Res 15:1359
63. Palareti G et al. (2016) Comparison between different D-Dimer cutoff values to assess the individual risk of recurrent venous thromboembolism: analysis of results obtained in the DULCIS study. Int J Lab Hematol 38:42–49
64. Tatarchuk TR et al. (2018) Effect of cobalt substitution on structural, elastic, magnetic and optical properties of zinc ferrite nanoparticles. J Alloy Compd 731:1256–1266
65. Gurav SK, Shirsath SE, Kadam RH, Mane DR (2013) Low temperature synthesis of Li0.5ZrxCoxFe2.5-2xO4 powder and their characterizations. Powder Technol 235:485–492
66. Hasani S et al. (2014) Nano/sub-micron crystallization of Fe-Co-7.15V alloy by thermo-mechanical process to improve magnetic properties. Mater Sci Eng B 190:96–103
67. Somaiah N, Jayaraman TV, Joy PA, Das D (2012) Magnetic and magnetoelastic properties of Zn-doped cobalt-ferrites - CoFe2-xZnxO4(x = 0, 0.1, 0.2, and 0.3). J Magn Magn Mater 324:2286–2291
68. Srinivasamurthy KM et al. (2018) Tuning of ferrimagnetic nature and hyperfine interaction of Ni2+ doped cobalt ferrite nanoparticles for power transformer applications. Ceram Int 44:9194–9203